APPLIED ORGANOMETALLIC CHEMISTRY
Appl. Organometal. Chem. **14**, 549–556 (2000)

EXAFS/XANES, chemisorption and IR investigations of colloidal Pt/Rh bimetallic catalysts†

K. Siepen,[1‡] H. Bönnemann,[1*] W. Brijoux,[1] J. Rothe[2§] and J. Hormes[2**]
[1]MPI für Kohlenforschung, Postfach 101353, D-45466 Mülheim/Ruhr, Germany
[2]Physikalisches Institut der Universität Bonn, Nussallee 12, D-531 15 Bonn, Germany

Bimetallic Pt/Rh heterogeneous catalysts based on nanoscaled colloids supported on activated charcoal have been shown to exhibit maximum activity in hydrogenation of butyronitrile at a composition of 10 atom% Pt and 90 atom% Rh in the metallic core. This synergetic effect has to be traced back to the special structure of the bimetallic nanoparticles as elucidated by X-ray spectroscopy and CO chemisorption. The surface of Pt/Rh particles was investigated by CO chemisorption combined with IR spectroscopy. It has been shown that a $Pt_{10}Rh_{90}$ colloid exhibits the maximum ability to chemisorb CO, compared with other compositions. Based on the detection of the different types of bonding of CO molecules to the metal surface and the EXAFS results, our measurements reveal surface enrichment of the Rh component. The surface structure of the particles, which varies with the elemental composition, and the presence of a Pt-dominated core influence the CO chemisorption ability as well as the hydrogenation efficiency of the Pt/Rh colloid catalysts. Copyright © 2000 John Wiley & Sons, Ltd.

1 INTRODUCTION

Metal colloids are particularly well suited for the preparation of highly active and selective hydrogenation and oxidation catalysts because of their narrow particle size distribution and small particles in the optimum range of 1–5 nm.[1–3] Their catalytic properties are often superior to those conventional catalysts. The specific synthesis of nanoparticles with a well-defined size distribution and a bi- or mono-metallic composition is independent of the influence of the support material, as the colloidal particles are pre-formed and can be deposited on various supports from organic or aqueous solution by simple adsorption.

In this work, the separate investigation of the active metal component according to the precursor concept[2] has been shown to be helpful in understanding the reasons for the superior behavior of the specific catalyst. In the case of bimetallic particles, effects caused by the special geometry of adsorption sites (ensemble effect) or electronic effects based on the alloying of two transition-metal species at the surface or within the particle core (ligand effect) have been attributed responsibility for higher catalytic activities compared with monometallic catalysts. X-ray absorption spectroscopy (XAS) has been proven to be a spectroscopic technique especially well suited for the investigation of the electronic and geometric structure of small metallic particles in the absence of well-defined crystal structures.[4,5] While this holds especially for the detailed analysis of the extended x-ray absorption fine structure (EXAFS) and its rich information content on structure parameters such as bonding lengths and coordination numbers,[6] the additional information exposed by the X-ray absorption near-edge structure (XANES) has often been disregarded.

* Correspondence to: H. Bönnemann, MPI für Kohlenforschung, Postfach 101353, D-45466 Mülheim/Ruhr, Germany.
** Correspondence to: J. Hormes, Physikalisches Institut der Universität Bonn, Nussallee 12, D-53115 Bonn, Germany.
† Presented at the XIIIth FECHEM Conference on Organometallic Chemistry, held 29 August–3 September 1999, Lisbon, Portugal.
‡ Present address: Condea Chemie GmbH, Fritz-Staiger- Str. 15, D-25541 Brunsbüttel, Germany.
§ Present address: Forschungszentrum Karlsruhe GmbH, INE, Postfach 3640, D-76021 Karlsruhe, Germany.
Contract/grant sponsor: BMBF, Bonn; Contract/grant number: 03D0007A2.

2 EXPERIMENTAL

Colloid synthesis

Under argon $RhCl_3$ and $PtCl_2$ (in quantities corresponding to 0, 10, 30, 50, 70, 90 and 100 mol% Rh) were suspended in dry tetrahydrofuran (THF). At 50 °C a 0.2 M solution of $N(octyl)_4BEt_3H$ in THF was added dropwise within 16 h with stirring. A black–brown solution was obtained. After addition of 2 ml dry acetone at room temperature the solution was stirred for 1 h. At 0.1 Pa all volatile organic material was evaporated, yielding a greasy black solid, which was readily soluble in THF, toluene and acetone. The raw product was dissolved in 2 ml diethyl ether (technical quality) and precipitated by addition of 50 ml absolute ethanol. After several hours of sedimentation the clear supernatant solution was decanted and the residue was dried for 16 h at 0.1 Pa. A black pyrophoric powder was obtained which is soluble in THF, toluene and acetone and had to be handled under an inert atmosphere.

CO chemisorption

CO chemisorption was conducted using a Micromeritics ASAP 2010 chemisorption system, applying the static method. Before the measurements the samples were degassed at 150 °C/10^{-4} Pa for 16 h to remove chemisorbed gases and water. They were then reduced *in situ* with hydrogen at 40 °C to remove surface oxides. The conditions of pretreatment had been optimized with rhodium (Rh) and Platinum (Pt) catalysts. The purity of the gases used was >99.99%. First, a chemisorption isotherm was recorded, followed by the measurement of a physisorption isotherm after 30 min of degassing at 35 °C and 10^{-4} Pa. The difference was used to calculate the volume of the chemisorbed gas.

C IR investigations

IR measurements were carried out with a Nicolet 7199 and Bruker IFS 48-FT-IR spectrometer. The samples were prepared as KBr pellets in the case of powders or between two KBr plates in the case of greasy substances. Generally, IR measurements were not conducted with supported catalysts, because in the case of oxidic supports the coordination mode of CO to the metal surface was influenced, while in the case of activated charcoal IR detection of CO was not possible. To eliminate these influences, the pure colloids were charged with CO in solution (THF) simply by bubbling CO gas through this solution for 30 min at ambient temperature. By means of *in-situ* IR and NMR investigations, it had been shown that this time is sufficient to generate a maximum coverage of the surface. After this procedure, the solvent was evaporated under vacuum (0.1 Pa).

X-ray absorption measurements

All sample preparation and measuring steps were carried out strictly under inert gas conditions in order to avoid any air contact of the finely dispersed metal particles. X-ray absorption spectra were recorded using synchrotron radiation from the *El*ectron *S*tretcher and *A*ccelerator ELSA[7] (Bonn University Institute of Physics). The accelerator was run at electron energies of 2.3 GeV (Rh) and 2.7 GeV (Pt), respectively, and at an average current of about 40 mA in storage ring mode. The method of inert gas sample handling for XAS measurements in the standard transmission technique has been described elsewhere.[8] Argon-filled ionization chambers (Pt L_{III}, 400 mbar; Rh L_{III}, 20 mbar) have been used for the detection of the primary and the transmitted beam intensity. For measurements at the Pt L_{III}-edge (11564 eV) the Lemonnier-type[9] X-ray monochromator was equipped with a pair of Ge<422> single crystals ($2d$ = 2.306 Å). The minimum step width of about 0.4 eV was used in the near-edge region (11550–11600 eV), while the spectra in the EXAFS region (11600–12200 eV) were recorded with a resolution of 0.8 eV/step. At the Rh L_{III}-edge (30$\overset{\circ}{4}$ eV) the use of InSb<111> crystals ($2d$ = 7.481 Å) gave a minimum step width of about 0.1 eV. Harmonic reduction has been performed at the Rh L_{III}-edge by detuning the parallel alignment of the monochromator crystals to 50% of the maximum beam intensity. For the calibration of the energy scale of the monochromator, the Pt $2p_{3/2}$ or the Rh $2p_{3/2}$ energy has been assigned to the first inflection point in the spectrum of a face-centered cubic (fcc)-Pt foil (2.5 μm) or an fcc-Rh foil (0.5 μm), respectively.

In order to compare the measured absorption curves quantitatively, a linear background was fitted to the pre-edge region (Pt L_{III}, 11450–11540 eV; Rh L_{III}, 2960–2990 eV) and then subtracted before normalization to the 'edge jump', i.e. the estimation of the height of the atomic background. The Pt L_{III} EXAFS measurements have been analyzed according to the standard least-squares fitting technique[10] using the program

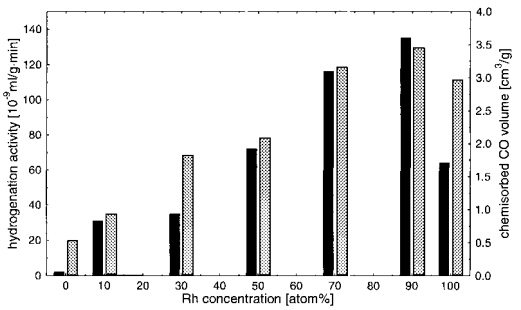

Figure 1 Correlation between CO chemisorption (gray bars) and butyronitrile hydrogenation activity (black bars) of Pt, Rh and Pt/Rh colloid catalysts.

package of Bertagnolli and co-workers.[11] For this analysis, theoretical phase and amplitude functions have been calculated with FEFF3.1.[12]

Catalytic test reaction

The procedure for hydrogenation of butyronitrile has been described elsewhere.[13]

3 RESULTS AND DISCUSSION

Catalysis and CO chemisorption experiments

Charcoal-supported bimetallic $Pt_mRh_n[N(octyl)_4Cl]$ colloids have been applied as catalysts in liquid-phase hydrogenation of butyronitrile to n-butylamine. It appears that the $Pt_{10}Rh_{90}$ bimetallic catalyst is the most active, which is not the case for a simple physical mixture with the same composition of monometallic Pt and Rh catalysts. Whereas the activity of the Pt catalyst (5% Pt on charcoal) is only 2 Nml H_2 (g catalyst)$^{-1}$ min^{-1} and that of the Rh catalyst (5% Rh on charcoal) is 64 Nml H_2 (g catalyst)$^{-1}$ min^{-1}, the $Pt_{10}Rh_{90}$ catalyst (5% metal on charcoal) exhibits an activity of 135 Nml H_2 (g catalyst)$^{-1}$ min^{-1}, which is more than double the performance of the Rh catalyst. In addition, the $Pt_{50}Rh_{50}$ and $Pt_{30}Rh_{70}$ catalysts had higher activities than the Rh catalyst, i.e. 72 and 116 Nml H_2 (g catalyst)$^{-1}$ min^{-1}, respectively. The CO chemisorption of this series of catalysts correlates well with the hydrogenation activities, as can be seen from Fig. 1. The $Pt_{10}Rh_{90}$ catalyst shows the highest CO chemisorption of 3.23 cm^3 (g catalyst)$^{-1}$ and the $Pt_{30}Rh_{70}$ catalyst the second highest of 2.96 cm^3 (g catalyst)$^{-1}$, whereas the Rh catalyst chemisorbs 2.78 cm^3 (g catalyst)$^{-1}$ (Fig. 1).

Table 1 Coordination modes of CO bonded to Pt and Rh surface atoms for colloid particles

Dicarbonyl	Linear	Bridged
CO—Rh^+—CO 2064 + 1988 cm^{-1}	Rh—CO 2004 cm^{-1} Pt—CO 2019 cm^{-1}	Rh—CO—Rh 1855 cm^{-1} Pt—CO—Pt 1800 cm^{-1}

The coordination number of CO to a mixed Pt/Rh surface of colloidal particles is unknown, because it depends on the composition and the type as well as the orientation of the surfaces exposed. Therefore, IR investigations of CO-covered Pt, Rh and bimetallic Pt_nRh_m colloids were carried out. In the case of Pt colloids, two species of CO coordinated to the Pt surface could be detected: a linearly bonded CO type with an absorption band at *ca* 2000 cm^{-1} and one with bridge-bonded CO with a

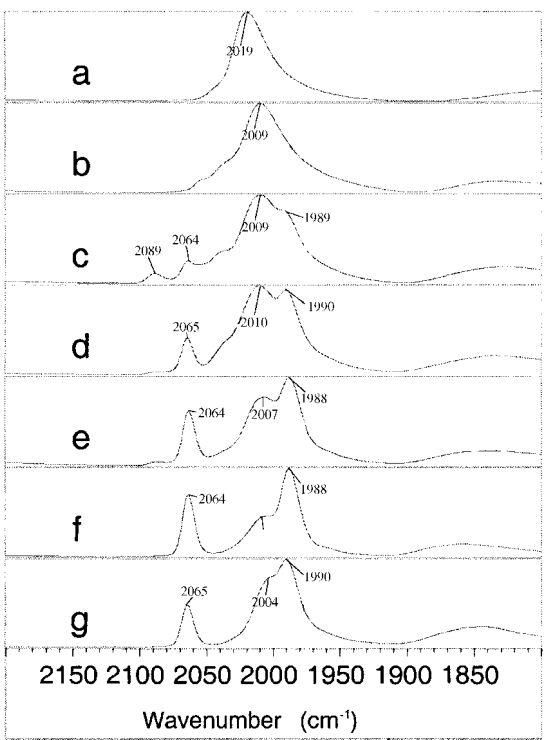

Figure 2 IR spectra of CO-covered Pt_mRh_n colloids; m/n = (a) 1:0; (b) 9:1; (c) 7:3; (d) 5:5; (e) 3:7; (f) 1:9 (g) 0:1.

broad absorption band at *ca*1800 cm^{-1}, which corresponds to results obtained with Pt single-crystal surfaces. In the case of the Rh and Pt/Rh colloids, a third type of CO coordination appears: a Rh–dicarbonyl species, where two CO molecules are bonded to one Rh atom, which has the formal charge of 1+.[14] Resonance repulsion causes the splitting of the absorption into two absorption bands at 2064 cm^{-1} and 1988 cm^{-1}, respectively (Table 1). This absorption is specific for Rh atoms present at the surface and is described in the literature for conventional supported Rh catalysts.[15] Its intensity increases with rising Rh content of the colloids. The $Pt_{10}Rh_{90}$ colloid exhibited the maximum intensity of dicarbonyl absorption (Fig. 2). This correlates with the results of CO chemisorption at supported Pt/Rh colloids. The ratio of dicarbonyl absorption and linear absorption is also influenced by the oxidation state of the surface Rh atoms. By an oxygen treatment before the CO loading, the number of Rh^+ centers at the surface can be enhanced, whereas a hydrogen treatment reduces them (Fig. 3). The IR spectra of CO-loaded Pt colloids are inert to oxygen or hydrogen treatment. There are no CO absorption bands detectable due to CO bound to Pt^+ or Pt^{2+}, which would be expected at *ca* 2100 cm^{-1}

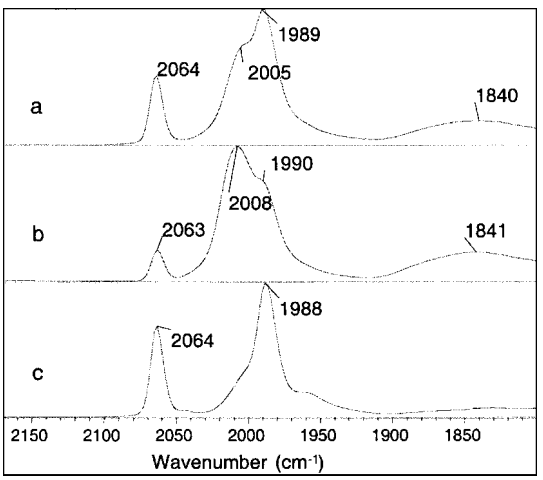

Figure 3 IR spectra of CO-covered Rh[N(octyl)$_4$] colloid: (a) without any pretreatment; (b) after hydrogen treatment; (c) after air treatment.

Pt L_{III} EXAFS

The EXAFS function and Fourier-filtered EXAFS of the Pt and Pt/Rh colloids are shown in Fig. 4. In order to demonstrate the quality of the data the EXAFS function as extracted by normalization to a polynomial function, i.e. to the unknown atomic background, has been given in the case of Pt_{100}. The Fourier-filtered first coordination shell EXAFS signals of $Pt_{70}Rh_{30}$, $Pt_{50}Rh_{50}$ and $Pt_{30}Rh_{70}$ indicate—by the characteristic beat structure—the presence of both Pt and Rh next-neighbors of Pt absorbers in the colloid particles. This has also been verified by the simulation of a comparable spectrum with FEFF7,[16] based on the assumption of a regular fcc structure with a random distribution of both metals. Significant changes in the k^3-weighted EXAFS-functions at different metal compositions of the colloid precursors can be observed. The Fourier transformations of the EXAFS functions are shown in Fig. 5. Again, the transformation of the EXAFS function as extracted has been given only for the Pt_{100} colloid. For all samples the transformation magnitude is dominated by a prominent structure between about 1 and 3 Å, comprising three more or less resolved peaks. As can be seen in Fig. 5 (top left), removal of noise—and possible contributions from more distant back-scatterers—do not significantly influence these

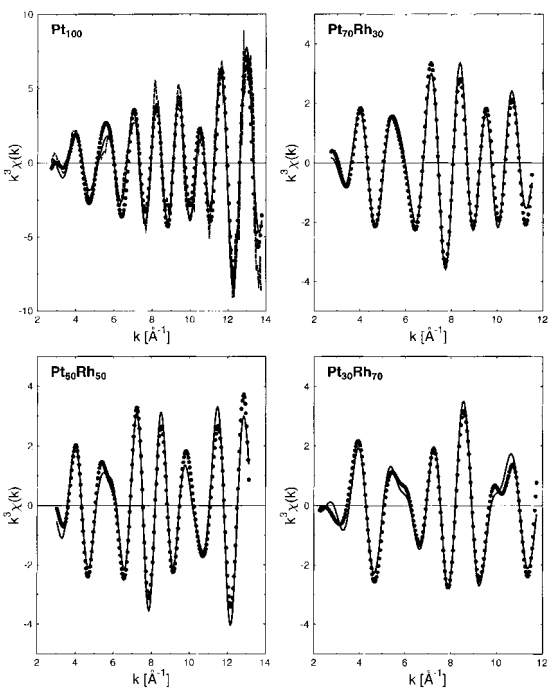

Figure 4 Pt L_{III} EXAFS: EXAFS function of the Pt colloid (—), Fourier filtered EXAFS functions (—) of the Pt and Pt/Rh colloids and best fits (●).

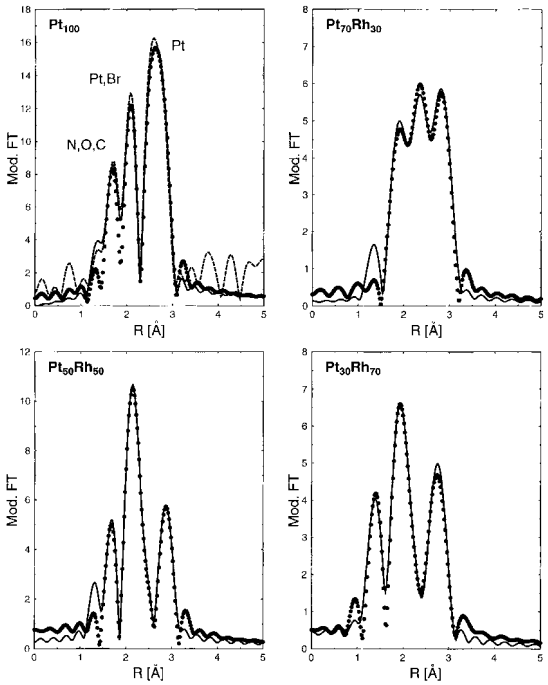

Figure 5 Pt L_{III} EXAFS: Fourier transformation of the EXAFS function of the Pt colloid (---), Fourier transformations of the filtered EXAFS functions (—) of the Pt and Pt/Rh colloids and best fits (●).

structures. In order to determine structural parameters from the EXAFS,[10] we have examined the reproducibility of the first shell filtered data by means of a two-shell fit using Pt and Rh backscatterers. The results obtained by the least-squares fitting procedure of the Fourier-filtered data are presented in Table 2. The error margins have been estimated following the method by Teo.[17] In agreement with the findings of several other authors, e.g. in the case of the investigation of PVP-stabilized Pt/Pd and Pt/Rh colloids by Toshima and co-workers[18,19] or the $N(butyl)_4$-protected Pt/Pd colloids by Kolb *et al.*,[20] it turned out that the two peaks at higher *R* values cannot be ascribed to either of the individual metals. This doublet structure is quite characteristic for the superposition of the amplitude and phase functions of both backscatterers. The first, less well defined peak above about 1 Å (30:70) or 1.5 Å (50:50, 70:30—disregarding the phase correction) can be traced back to the presence of one or more light backscatterers (N, O, C) at a distance of about 2 Å. Considering these contributions, which are missing in the spectrum of the metal foil, significantly improves the fit in the low-*k* region. Moreover, in the case of the $Pt_{70}Rh_{30}$ sample, this peak, due to the light backscatterers, cannot be safely separated from the signal of the metal backscatterers. A similar peak was observed in the case of monometallic $Pt[N(octyl)_4]^+$ (Fig 5 top left, Table 2). Probably as a consequence of the superposition of the influence of the two metals, no contribution of the halogenide to the EXAFS has been detected for the bimetallic colloids. Note that in the case of the pure Pt colloid the Br signal is superimposed on the side lobe due to the Ramsauer–Townsend modulation of the Pt backscattering amplitude.[21]

First, a remarkable decrease in the first shell coordination number of 12 for Pt atoms in the fcc-type lattice to about half that value for Pt in Pt and Pt/Rh colloids has been found. This result cannot be explained solely by assuming a high degree of surface atoms with missing next-neighbors in the

Table 2 Structure parameters and estimated error margins derived from EXAFS analysis of the Pt and Pt/Rh colloids

Colloid	Backscat.	$R \pm 0.01$ (Å)	$N \pm 0.5$	$\sigma^2 \pm 0.002$ (Å^2)	$\Delta E_0 \pm 1$ (eV)
$Pt_{30}Rh_{70}$	Pt	2.65	3.4	0.0048	−2
	Rh	2.65	1.7	0.0049	6
	N	1.82	0.4	4.0E-8	−7
$Pt_{50}Rh_{50}$	Pt	2.71	4.5	0.0071	7
	Rh	2.69	1.3	0.0026	6
	O	2.02	0.4	2.0E-7	8
$Pt_{70}Rh_{30}$	Pt	2.71	6.0	0.0088	6
	Rh	2.70	1.2	0.0096	8
	N	2.11	0.3	6.0E-7	4
Pt_{100}	Pt	2.75	5.9	0.0066	9
	Br	2.44	0.2	2.5E-7	−2
	O	2.00	0.8	1.0E-8	12

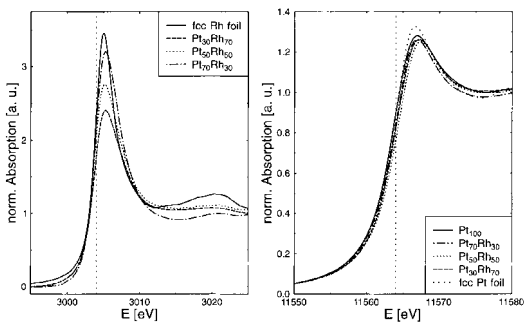

Figure 6 Left: Rh L_{III} XANES of fcc Rh and the Pt/Rh colloids. Right: Pt L_{III} XANES of fcc Pt and the Pt and Pt/Rh colloids.

colloid particles. An idealized four-shell Pt or Rh cluster of about 2.2 nm diameter would exhibit about 50% of the atoms in surface positions, leading to an average coordination number which is close to 10. What seems to be as likely is the influence of static as well as dynamic disorder, i.e. the presence of a large fraction of 'ill-coordinated' Pt atoms in the severely distorted and highly fluxional nanoscale lattice. This explanation has been given by Di Cicco *et al.*[22] to explain the decrease in coordination numbers in ball-milled nanometer iron particles derived by EXAFS. In the case of bimetallic alloy particles, a cumulant analysis to evaluate the influence of thermal or static disorder on the coordination number is complicated due to the fact that the first-shell pair distributions are not monoatomic.[23] However, several authors, e.g. Boyanov and Morrison in their study of zeolite-supported platinum clusters containing only 10–25 Pt atoms on average,[24] have shown identical results for a cumulant analysis compared with the standard method, static disorder in their case thus being symmetric on average.

Secondly, only a slight decrease in the interatomic distance has been found in the case of colloidal Pt (2.75 Å vs. 2.77 Å bulk value), whereas the nanoscale alloying yields Pt–Pt and Pt–Rh next-neighbor distances which are close to the Rh bulk value of 2.69 Å for $Pt_{70}Rh_{30}$ and $Pt_{50}Rh_{50}$. As already mentioned above, it is well known that the standard EXAFS analysis of nanometer-scale metal particles may lead to the underestimation of atomic distances caused by disregard of the anharmonic movement of a large fraction of the surface atoms. On the other hand, molecular dynamics simulations point to the adjustment of the bulk value of the next-neighbor distance, when metal clusters of diameters of more than 2 nm are considered.[25] Consequently, the difference of 0.02 Å between the Pt bulk value and the corresponding fit parameter obtained in the case of the monometallic colloid can be regarded as a good estimate of the maximum distance error due to the standard analysis.

Interestingly, in the case of $Pt_{30}Rh_{70}$ an even lower distance of 2.65 Å has been found for both Pt and Rh backscatterers, indicating a somewhat stronger lattice contraction when the colloid particular contain excess Rh. Looking at the ratio of the first-shell Pt and Rh coordination numbers, it becomes clear that no random distribution of the metals results from co-reduction of the respective halogenides. As has been shown also by IR measurements on chemisorbed CO, Rh is enriched at the surface, giving rise to a higher Pt concentration in the center of the bimetallic particles. Nevertheless, the presence of light elements—probably belonging to the surfactant shell or to a surface oxide layer—as next-neighbors to Pt absorbers has been reported. Thus a complete segregation of both components, i.e. the formation of a closed shell of Rh atoms surrounding a pure Pt core (as postulated by Toshima for PVP-protected Pt/Pd colloids) is rather unlikely. In the $Pt_{30}Rh_{70}$ sample the Rh concentration in the core seems to be sufficient to give rise to a more homogeneous structure with equal Pt–Pt and Pt–Rh distances. This special structure may also be responsible for the increased catalytic activity of these particles, as compared with pure Rh colloids.

Rh L_{III} and Pt L_{III} XANES

The normalized Rh L_{III} and Pt L_{III} XANES spectra of the Pt and Pt/Rh colloids are presented in Fig. 6 in the region of the L_{III} resonances ($2p_{3/2} \rightarrow 4d_{5/2}$ and $2p_{3/2} \rightarrow 5d_{5/2}$ transitions respectively). In both sets of measurements the maxima of the white lines of the bimetallic samples are shifted only slightly to higher energies (Rh, 0.2 eV; Pt, 0.5 eV) compared with the spectra of the respective metal foils. Whereas the measurements of the colloids at the Pt edge reveal no significant deviations of the intensity and of the area of the resonances from each other, the influence of the ratio of the metal concentrations is quite obvious at the Rh edge. Here the resonances show a decreasing intensity with increasing Rh concentration, while the spectrum of the metal foil exhibits the most intense white line. Considering the similar results of Sinfelt *et al.* for bimetallic Os/Cu clusters,[6] the varying intensity of the Rh L_{III} white line can be interpreted as due to the

increasing charge transfer from the Rh component to the Pt component with decreasing Rh content in the particles. This conclusion is also supported by the interpretation of the transition-metal L XANES given by Sham[26] or Mansour,[27] who ascribe the white line intensity to the density of unfilled *d*-like electronic states at the Fermi level scanned by the excited $2p_{3/2}$ electrons. In the case of the Pt/Rh[$N(octyl)_4^+$] colloids, it is reasonable to assume that in spite of the metal segregation the increasing Rh content leads also to the enrichment of this component in the Pt-dominated cores of the colloid particles. Consequently, a larger fraction of the Rh atoms interacts directly with Pt atoms, thus forming a nanoscale alloy (see also the EXAFS results for $Pt_{30}Rh_{70}$). Accordingly, in the case of $Pt_{70}Rh_{30}$ the electronic state of the Rh atoms enriched at the surface is rather similar to that of Rh metal, i.e. the Rh XANES is dominated by the larger fraction of Rh surface atoms.

The shifts of the Rh L_{III} and the Pt L_{III} white lines are close to the energy step witdths of 0.1 eV and 0.4 eV at the Rh and the Pt L_{III}-edge, respectively, but they all point in the same direction. The broadening of the white lines and the shift to higher energies can be traced back to the presence of Rh atoms or Pt atoms, respectively, in a non-zerovalent state due to the interaction with chemisorbed oxygen or halogenides (compare with the IR measurements). As can be deduced from the ratio of next-neighbor coordination numbers found by EXAFS, even in the case of excess Rh concentration the Pt absorbers are predominantly coordinated by Pt backscatterers. Thus, on average the electronic influence of the Rh componrents remains weak at the Pt L_{III}-edge.

4 CONCLUSIONS

Considering the low next-neighbor distance of 2.65 Å obtained for our $Pt_{30}Rh_{70}$ alloy colloid, the improved performance of the corresponding catalyst seems to be due more to the geometric (ensemble) effect of the special particle structure present when an excess Rh concentration is present. Nevertheless, from our CO chemisorption experiments, we conclude that Pt atoms influence the charge density of Rh atoms at the surface of the nanosized particles, as all our measurements otherwise point to a surface enrichment of the Rh component for all Pt/Rh compositions (note that in the case of bulk alloys the Pt component tends to segregate and be enriched at the surface). Partial oxidation of the Rh surface atoms is certainly caused by traces of oxygen, which are present even when working under inert gas atmosphere, and thus give rise to the formation of the characteristic Rh^+ dicarbonyl species. Nevertheless, our XANES measurements point to the fact that Pt core atoms are capable of drawing electrons from the Rh surface atoms, leading to an additional ligand effect which also might explain the superior performance of the $Pt_{30}Rh_{70}$- $Pt_{10}Rh_{90}$-derived catalysts.

Acknowledgement We gratefully acknowledge the financial support of the BMBF, Bonn, under Contract No. 03D0007A2.

REFERENCES

1. Bönnemann H, Brijoux W. In *Active Metals*, Fürstner A, (ed.). VCH: Weinheim, 1996.
2. Bönnemann H, Brijoux W. In *Advanced Catalysts and Nanostructured Materials*, Moser WR (ed.). Academic Press: New York, 1996.
3. Bönnemann H, Brijoux W, Richter J, Becker R, Hormes J, Rothe J. *Z. Naturforsch., B* 1995; **50**(3):333–338.
4. Franke R, Rothe J, Pollmann J, Hormes J, Bönnemann H, Brijoux W, Hindenburg Th. *J. Am. Chem. Soc.* 1996; **118**: 12090–12097.
5. Rothe J, Hormes J, Bönnemann H, Brijoux W, Siepen K. *J. Am. Chem. Soc.* 1998; **120**: 6019–6023.
6. Sinfelt H, Via GH, Lytle FW. *Catal. Rev.—Sci. Eng.* 1984; **26**(1):81–140.
7. Althoff KH, Drachenfels Wv, Dreist A, Husmann D, Neckening M, Nuhn HD, Schauerte W, Schillo M, Schittko FJ, Wermelskirchen C. *Particle Accel.* 1990; **27**: 101–106.
8. Rothe J, Franke R, Pollmann J, Hormes J, Bönnemann H, Brijoux W, Siepen K, Richter J. *Fresenius' J. Anal. Chem.* 1996; **355**: 372–374.
9. Lemonnier M, Collet O, Depautex C, Esteva JM, Raoux D. *Nucl. Instrum Methods* 1987; **152**: 109.
10. Koningsberger DC, Prins R (eds). *X-Ray Absorption: Techniques of EXAFS, SEXAFS and XANES*. John Wiley: New York, 1988; 211–253.
11. Ertel TS, Bertagnolli H, Hückmann S, Kolb U, Peter D. *Appl. Spectosc.* 1992; **46**(4): 690–698.
12. Mustre de Leon J, Rehr JJ, Zabinsky SI, Albers RC. *Phys. Rev. B* 1991; **44**(9): 4146–4156.
13. Bönnemann H, Brijoux W, Brinkmann R, Dinjus E, Fretzen R, Joußen T, Korall B. *J. Mol. Catal.* 1992; **74**: 323–333.
14. van't Blik HFJ, van Zon JBAD, Huizinga T, Vis JC, Koningsberger DC, Prins R. *J. Am. Chem. Soc.* 1985; **107**: 3139–3147.
15. Solymosi F, Pasztor M. *J. Phys. Chem.* 1986; **90**: 5312.
16. Zabinsky SI, Rehr JJ, Ankudinov A, Albers RC, Eller MJ. *Phys. Rev. B* 1995; **52**: 2995.

17. Teo B-K. *EXAFS: Basic Principles and Data Analysis*. Springer: Berlin, 1986; 132–133.
18. Toshima N, Harada M, Yonezawa T, Kushihashi K, Asakura K. *J. Phys. Chem.* 1991; **95**: 7448–7453.
19. Harada M, Asakura K, Toshima N. *J. Phys. Chem.* 1994; **98**: 2653–2662.
20. Kolb U, Quaiser A, Winter M, Reetz MT. *Chem. Mater.* 1996; **8**: 1889–1894.
21. Teo B-K, Lee PA. *J. Am. Chem. Soc.* 1979; **101**: 2815–2832.
22. Di Cicco A, Berrettoni M, Stizza S, Bonetti E. *Physica B*;1995 **208–209**: 547–548.
23. Dalba G, Fornasini P, Rocca F. *Phys. Rev. B* 1993; **47**(14): 8502–8514.
24. Boyanov BI, Morrison TI. *J. Phys. Chem.* 1996; **100**: 16310–16317.
25. Clausen BS, Topsoe H. *Jpn. J. Appl. Phys.* 1993; **32**: 95–98.
26. Sham TK. *Phys. Rev. B* 1985; **31**(4): 1903–1908.
27. Mansour AN, Cook JW Jr, Sayers DE. *J. Phys. Chem.* 1984; **88**: 2330–2334.

